Sensorless PM Brushless DC Motor Drives

Nobuyuki Matsui

Abstract— **To control PM brushless dc motors, position and speed sensors are indispensable because the current should be controlled depending on the rotor position. However, these sensors are undesirable from standpoints of size, cost, maintenance, and reliability. There are different ways of approaching this problem, depending on the flux distribution. The paper presents the speed and position sensorless control of PM brushless dc motors with a sinusoidal flux distribution. Two approaches are presented and compared with each other; one is based on the voltage model of the motor and another is based on the current model. The starting procedure is also a very difficult problem under sensorless drives, because the sensorless drive algorithm uses voltage and current for estimation of rotor position, but no information is available before starting. A novel starting method is presented by using a salient-pole machine. Experimental results based on DSP-TMS320C25 controller are shown for comparisons, which demonstrate desired characteristics both in steady-state and starting condition.**

I. Introduction

GENERALLY, the high performance ac variable drive requires speed/position sensors. The vector-controlled induction motor basically uses a speed sensor and the PM brushless dc motor requires a position sensor with which commutation and current control are performed. However, the rotor position sensor and the speed sensor present several disadvantages from the standpoint of drive cost, machine size, reliability, and noise immunity. For this reason, it is desired to eliminate these sensors from the motor, that is, a sensorless control of the brushless dc motor is expected. The brushless dc motor can be classified from the standpoint of its flux distribution, trapezoidal or sinusoidal flux distribution, and the sensorless control strategy is different depending on it.

The brushless motor with a trapezoidal flux distribution provides an attractive candidate for the sensorless operation because two of three windings are excited at a time. Therefore, the unexcited winding can be used as a sensor. The typical and well-known method is to detect an induced EMF in the winding [1]–[4]. Another ingenious method is based on the detection of on/off state of the switching devices of the inverter to determine a commutation instant [5], [6]. However, this kind of motor presents relatively high levels of torque ripple and the applications are restricted.

On the contrary, the brushless motor with a sinusoidal flux distribution excites three windings at a time, and therefore, a sensorless control algorithm becomes complicated. Several approaches have been proposed, for example, by using the state observer [7] and the extended Kalman filter [8]. They showed a feasibility of sensorless drive of a PM synchronous motor but the operating characteristics were not fully examined. In this paper, two approaches to the sensorless operation of brushless motors with a sinusoidal flux distribution are presented. The basis of the proposed sensorless control algorithm is to use differences between the detected actual state variables and the estimated state variables which are calculated from an equivalent motor model in the controller. Therefore, the approach is different depending on the type of the motor model, the voltage model, and the current model.

Unlike the sensorless drives of vector-controlled induction motors, the starting procedure of sensorless drives of PM brushless motors is difficult. Since the rotor has a permanent magnet and there is no information on the rotor position before starting, the application of rotating field at an arbitrary position may be accompanied with a temporary reverse rotation or may lead to a starting failure. As the starting procedure, starting from a predetermined rotor position [9], [10] and the open-loop control from standstill to the speed at which the rotor position can be reliably calculated by using state variables [11] have been reported. The salient-pole brushless dc motor is attractive to solve this problem. Since the winding inductance is a function of the rotor position, the rotor position at standstill can be estimated by a proper detection of the winding inductances.

The proposed control schemes were verified by experiments using a 1.2-kW PM brushless dc motor with a cylindrical rotor and 2.2-kW PM motor with a salient rotor.

II. Brushless DC Motor Model

Fig. 1 shows an analytical model of a brushless motor with a PM sinusoidal flux excitation, where d-q axis corresponds to the actual rotor position and γ-δ axis is the assumed rotor position with an angular error $\Delta\theta$ given in (1) with respect to the actual rotor position:

$$\Delta\theta = \theta - \theta_c. \tag{1}$$

The voltage equation is given in (2), where R_a, L_a; armature winding resistance and inductance, K_3; EMF constant, i_u, i_v, i_w; line currents, v_u, v_v, v_w; phase voltages and p is a derivative operator:

$$\begin{bmatrix} v_u \\ v_v \\ v_w \end{bmatrix} = \begin{bmatrix} R_a + pL_a & L_a\cos(2\pi/3) & pL_a\cos(4\pi/3) \\ pL_a\cos(4\pi/3) & R_a + pL_a & pL_a\cos(2\pi/3) \\ pL_a\cos(2\pi/3) & pL_a\cos(4\pi/3) & R_a + pL_a \end{bmatrix} \times \begin{bmatrix} i_u \\ i_v \\ i_w \end{bmatrix} + K_3 p \begin{bmatrix} \cos\theta \\ \cos(\theta - 2\pi/3) \\ \cos(\theta + 2\pi/3) \end{bmatrix}. \tag{2}$$

Under the conventional control, voltages and currents in (2) are transformed to the actual d- and q-axis values to

Manuscript received June 1, 1995; revised November 8, 1995.

The author is with the Department of Electrical and Computer Engineering, Nagoya Institute of Technology, Nagoya 466, Japan.

Publisher Item Identifier S 0278-0046(96)02362-3.

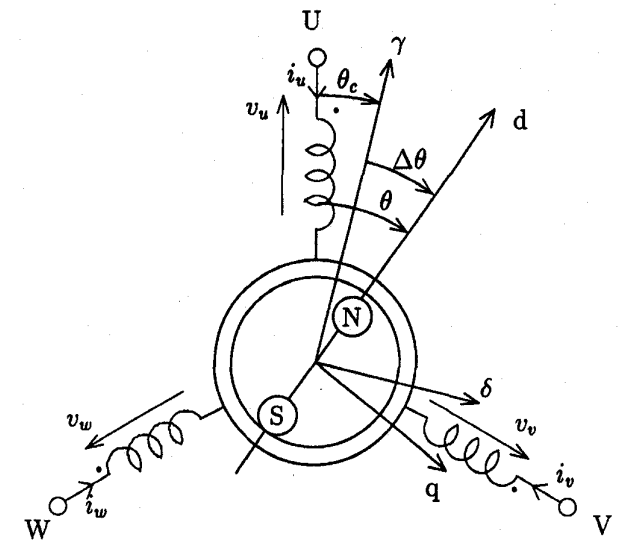

Fig. 1. Analytical model of PM brushless dc motor.

obtain an equivalent two-axis model by using the known rotor position angle. However, the actual rotor position is unknown under the sensorless drive and voltages and currents should be transformed by the transformation matrix in (3) which is based on the assumed rotor position angle:

$$\begin{bmatrix}\gamma\\ \delta\end{bmatrix} = \sqrt{\frac{2}{3}}\begin{bmatrix}\cos\theta_c & \cos(\theta_c-2\pi/3) & \cos(\theta_c+2\pi/3)\\ -\sin\theta_c & -\sin(\theta_c-2\pi/3) & -\sin(\theta_c+2\pi/3)\end{bmatrix} \times \begin{bmatrix}u\\ v\\ w\end{bmatrix}. \tag{3}$$

As a result, the γ-δ axis voltage equation of the brushless motor is given in (4). By following the conventional control, γ-axis current is controlled to be zero and the generated torque is given in (5).

$$\begin{bmatrix}v_\gamma\\ v_\delta\end{bmatrix} = \begin{bmatrix}R+pL & -L\dot\theta_c\\ L\dot\theta_c & R+pL\end{bmatrix}\begin{bmatrix}i_\gamma\\ i_\delta\end{bmatrix} + K_E\dot\theta\begin{bmatrix}-\sin\Delta\theta\\ \cos\Delta\theta\end{bmatrix} \tag{4}$$

$$K_E = \sqrt{\frac{3}{2}}K_3,\ \dot\theta = \frac{d\theta}{dt},\ \dot\theta_c = \frac{d\theta_c}{dt},\ R = R_a, L = (3/2)L_a$$
$$\tau = K_T i_\delta \cos\Delta\theta. \tag{5}$$

Fig. 2 shows a schematic diagram of the sensorless drive of a PM brushless dc motor. Speed and position are estimated in an estimator block by using voltages and currents. Here, currents are detected by a current sensor which is very common in the conventional control system of a brushless motor. Voltages are obtained by calculation, not by detection, by using information on PWM pattern, dc voltage, and dead time. This is very important because no additional sensor is necessary for the sensorless drive. The estimated speed is compared to the speed reference and the speed error is processed in the PI speed regulator to obtain the torque component of current reference i_δ^* while the γ-axis current reference is zero as previously explained. The current controller is designed on the basis of γ-δ model and the estimated position is used to perform

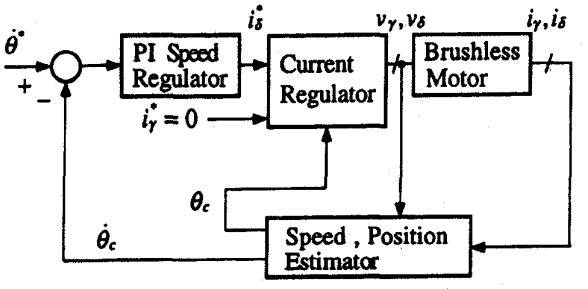

Fig. 2. Sensorless control block diagram.

the transformation from three phase voltages and currents to corresponding two-axis values.

III. Voltage Model-Based Control Algorithm [12]

Based on the voltage equation (4), the rotor position and speed can be estimated in the following manner. Assuming the ideal condition that $\Delta\theta = 0$ and $\dot\theta_c = \dot\theta$, (4) can be rearranged as in (6)

$$\begin{bmatrix}v_{\gamma M}\\ v_{\delta M}\end{bmatrix} = \begin{bmatrix}R+pL & -L\dot\theta\\ L\dot\theta & R+pL\end{bmatrix}\begin{bmatrix}i_\gamma\\ i_\delta\end{bmatrix} + K_E\dot\theta\begin{bmatrix}0\\ 1\end{bmatrix}. \tag{6}$$

From (6), the hypothetical speed $\dot\theta_e(=\dot\theta_c = \dot\theta)$ can be obtained by the following relation:

$$\dot\theta_e = \frac{v_{\delta M} - (R+pL)i_\delta}{K_E + Li_\gamma}.$$

From the assumption that $\Delta\theta = 0$,

$$v_{\delta M} = v_\delta$$

can be deduced and the hypothetical speed is given as follows:

$$\dot\theta_e = \frac{v_\delta - (R+pL)i_\delta}{K_E + Li_\gamma}. \tag{7}$$

In the actual operating condition, $\Delta\theta \neq 0$, $\dot\theta_c \neq \dot\theta$, the corresponding correction of the hypothetical speed is necessary. The correction is performed based on the γ-axis component.

The γ-axis applied voltage $v_{\gamma M}$ under an ideal condition ($\Delta\theta = 0$, $\dot\theta_e = \dot\theta_c = \dot\theta$) is given as follows:

$$v_{\gamma M} = (R+pL)i_\gamma - L\dot\theta_e i_\delta. \tag{8}$$

Here, $v_{\gamma M}$ is a hypothetical voltage but it can be calculated using the actual current transformed by (3). Since v_γ in (4) can be also obtained after transforming the actual applied voltage to γ-δ axis voltage by (3), the γ-axis voltage difference can be obtained as follows:

$$\Delta v_\gamma = v_\gamma - v_{\gamma M} = -\dot\theta K_E \sin\Delta\theta. \tag{9}$$

Assuming that $\dot\theta \neq 0$ and $\Delta\theta \cong 0$, (9) can be approximated as follows:

$$\Delta v_\gamma \cong -K_E\dot\theta\Delta\theta. \tag{10}$$

The above equation means that the voltage difference is proportional to the angular difference between the assumed and the actual rotor axes. Using (7) and (10), the following estimation algorithm results.

For the clockwise rotation

if $\Delta v_\gamma > 0 (\Delta\theta < 0)$, then $\dot{\theta}_c$ should be decreased.

if $\Delta v_\gamma < 0 (\Delta\theta < 0)$, then $\dot{\theta}_c$ should be increased.

For the counterclockwise rotation

if $\Delta v_\gamma > 0 (\Delta\theta < 0)$, then $\dot{\theta}_c$ should be increased.

if $\Delta v_\gamma < 0 (\Delta\theta > 0)$, then $\dot{\theta}_c$ should be decreased.

According to the above algorithm, the hypothetical speed in (7) should be corrected. There are many ways to obtain the correction speed n_W. The following is a simple implementation using the conventional PI control

$$n_W = -\sin(\dot{\theta}_e)\left(K_{SP}\delta v_\gamma + K_{SI}\int \Delta v_\gamma dt\right).$$

Here K_{SP} and K_{SI} are the gains of PI controller, respectively. Using this correction speed, the speed can be obtained as follows:

$$\dot{\theta}_c = \dot{\theta}_e + n_W. \tag{11}$$

IV. Current Model-Based Control [10]

In this control algorithm, estimation of the position and speed is performed using a current error between an actual current and the model current obtained from a current model of the motor. Rearranging (4), the current model of the brushless motor is given in (12)

$$\begin{aligned} p\begin{bmatrix} i_\gamma \\ i_\delta \end{bmatrix} &= \frac{1}{L}\left[\begin{bmatrix} v_\gamma \\ v_\delta \end{bmatrix} - \begin{bmatrix} R & -L\dot{\theta}_c \\ L\dot{\theta}_c & R \end{bmatrix}\begin{bmatrix} i_\gamma \\ i_\delta \end{bmatrix} - K_E\dot{\theta}\begin{bmatrix} -\sin\Delta\theta \\ \cos\Delta\theta \end{bmatrix}\right] \\ &= \frac{1}{L}\left[\begin{bmatrix} v_\gamma \\ v_\delta \end{bmatrix} - \begin{bmatrix} R & -L\dot{\theta}_c \\ L\dot{\theta}_c & R \end{bmatrix}\begin{bmatrix} i_\gamma \\ i_\delta \end{bmatrix} - e\begin{bmatrix} -\sin\Delta\theta \\ \cos\Delta\theta \end{bmatrix}\right] \end{aligned} \tag{12}$$

where $e = K_E\dot{\theta}$ is an EMF of the actual motor.

Suppose that currents at any sampling point are i_γ^n and i_δ^n, then currents at the next sampling point i_γ^{n+1}, i_δ^{n+1} are approximately given by the following relation under the assumption that the current sampling period is short enough compared to the time constant of armature current:

$$\begin{bmatrix} i_\gamma^{n+1} \\ i_\delta^{n+1} \end{bmatrix} = \begin{bmatrix} i_\gamma^n \\ i_\delta^n \end{bmatrix} + p\begin{bmatrix} i_\gamma \\ i_\delta \end{bmatrix}T. \tag{13}$$

Here, T is the sampling period. Equations (12) and (13) are valid for an actual motor.

The current model of the motor is in the controller. In the model, the assumed and actual axes are coincident. As a result, the current model is given in (14) and (15), where e_c is the motor EMF of the model

$$p\begin{bmatrix} i_{\gamma M} \\ i_{\delta M} \end{bmatrix} = \frac{1}{L}\left[\begin{bmatrix} v_\gamma \\ v_\delta \end{bmatrix} - \begin{bmatrix} R & -L\dot{\theta}_c \\ L\dot{\theta}_c & R \end{bmatrix}\begin{bmatrix} i_\gamma \\ i_\delta \end{bmatrix} - e_c\begin{bmatrix} 0 \\ 1 \end{bmatrix}\right] \tag{14}$$

$$\begin{bmatrix} i_{\gamma M}^{n+1} \\ i_{\delta M}^{n+1} \end{bmatrix} = \begin{bmatrix} i_\gamma^n \\ i_\delta^n \end{bmatrix} + p\begin{bmatrix} i_{\gamma M} \\ i_{\delta M} \end{bmatrix}T. \tag{15}$$

The current error between the actual motor current and the model current is obtained from (12–15) and the following relation results:

$$\begin{bmatrix} \Delta i_\gamma^{n+1} \\ \Delta i_\delta^{n+1} \end{bmatrix} = \begin{bmatrix} i_\gamma^{n+1} - i_{\gamma M}^{n+1} \\ i_\delta^{n+1} - i_{\delta M}^{n+1} \end{bmatrix} = \frac{T}{L}\begin{bmatrix} e\cdot\Delta\theta \\ -(e-e_c) \end{bmatrix}. \tag{16}$$

Here, the following assumptions are used:

$$\sin\Delta\theta \cong \Delta\theta, \quad \cos\Delta\theta \cong 1. \tag{17}$$

From (16), the following assumptions are deduced.

A. δ-axis current error is proportional to the difference between the actual and model emfs.

B. γ-axis current error is proportional to the angular error.

From A, the model EMF can be obtained by using δ-axis current error and

$$e_c^{n+1} = e_c^n - K_e\Delta i_\delta^n. \tag{18}$$

From B and (18), the position can be obtained in (19):

$$\theta_c^{n+1} = \theta_c^n + \frac{e_c^{n+1}}{K_E}T + K_\theta\Delta i_\gamma^n. \tag{19}$$

Since the speed is a derivative of the position, it can be obtained by using (19):

$$\dot{\theta}_c^{n+1} = \frac{\theta_c^{n+1} - \theta_c^n}{T} = \frac{e_c^{n+1}}{K_E} + \frac{K_\theta}{T}\Delta i_\gamma^n. \tag{20}$$

Here, K_e, K_θ are estimation gains.

The current model-based sensorless control algorithm does not use voltage information. This fact means that the control is free from the inaccuracy of voltage caused by an inverter. The dead time, voltage drop across the switching devices and dc voltage variation do not cause a serious effect on the control characteristics.

V. Experimental System

The experimental system configuration is shown in Fig. 3. The six-pole, 1.2-kW, permanent magnet type brushless dc motor, whose specifications are given in Table I, is used. DSP-TMS320C25 performs all necessary control processings and the sampling time is 200 μs. The current is detected by a Hall-CT and is converted through a 12-bit A/D converter with a resolution of 2.2×10^{-2} A/bit. As previously explained, the applied voltage is obtained by calculation, not by detection, using the dc voltage, PWM pattern, and the dead-time information. The dc voltage, obtained through a capacitor-input diode bridge circuit connected to a 3-phase, 200-V commercial source, is detected as a 12-bit quantity through a V/F converter with a resolution of 0.137 V/pulse.

VI. Experimental Results

Fig. 4 shows the steady state operating characteristics under a voltage model-based sensorless control algorithm. In Fig. 4(a), a comparison between the actual rotor position monitored by a resolver and the estimated position under the voltage model-based control algorithm is shown. Both position traces show a good agreement. In Fig. 4(b) the steady state

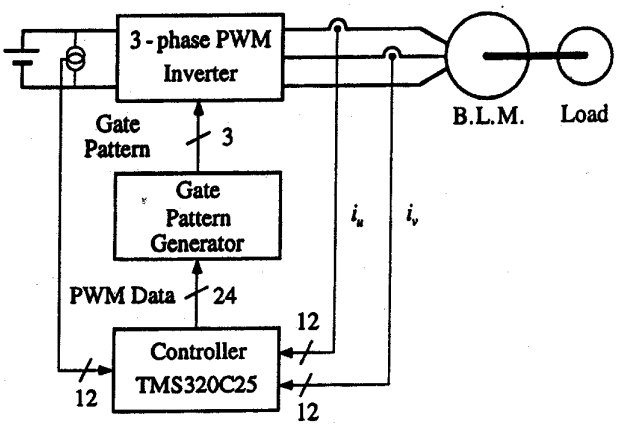

Fig. 3. Experimental system configuration.

TABLE I
SPECIFICATIONS OF TEST MOTOR

no. of poles	6
rated output	1.2 *kW*
rated voltage	164 *V*
rated curr.	5 *A*
rated speed	1200 *rpm*
rated torque	98 *kgfcm*
rotor inertia	77.6 $kgfcm^2$
friction coneff.	4.04×10^{-3} m^2/s
armature resis.	1.91 Ω
arm. inductance	9.55 *mH*
torque const.	0.332 *Nm/A*

torque-speed characteristics are shown. The speed range is 100 ~ 1200 r/min with a load torque variation from 0% to 100%. In this operating condition, the steady state maximum speed error is within 1%.

Below 100 r/min, the speed fluctuation became larger and a stable rotation could not be obtained. The instability below 100 r/min is explained by two reasons. One reason is a current ripple. Since the current ripple increases with a decrease of speed, a variation of the estimated speed calculated in (7) increases. To avoid this problem, a moving average over eight current samplings was used. Another very significant reason is a voltage control accuracy of the inverter. In the lower speed range, the applied voltage to the motor also becomes lower and the effect of dead time, the voltage drop across the switching devices and power feeder are becoming more significant. The dead time was compensated for by control software of the inverter but the voltage drops across the switching devices were not compensated for in the experimental system.

Fig. 5 shows a similar steady state operating characteristics under a current model-based algorithm. Fig. 5(a) and (b) shows the estimated speed and position at a 1200-r/min speed reference under the rated load. In Fig. 5(a), the motor parameter is coincident with that of the model and a model speed and the estimated position show good agreements with

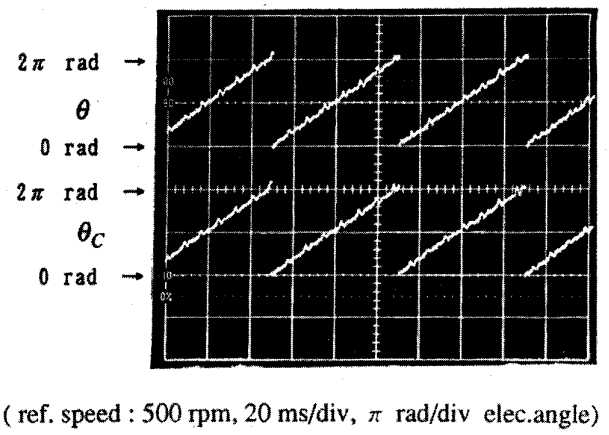

(a)

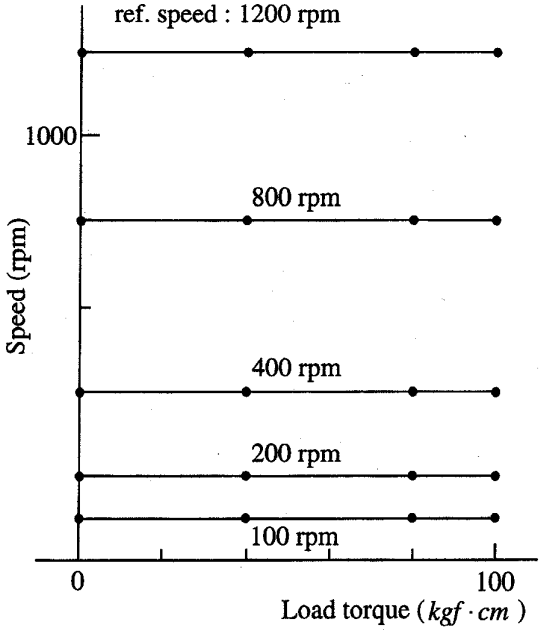

(b)

Fig. 4. Steady-state operating characteristics under voltage model-based control. (a) Comparison of position between actual and estimated values. (b) Torque-speed characteristics.

their respective references. In Fig. 5(b), the EMF constant of the model is 1.25 times the actual EMF constant, but the axis speed and the estimated position show good agreement with their respective references. This experiment corresponds to the case where the EMF constant is decreased due to the negative temperature coefficient of ferrite magnet.

The same experiments were performed to examine the effect of error in inductance on speed and position estimations and the results showed a robustness of estimation against parameter differences between a model and an actual motor.

In Fig. 5(c) the torque-speed characteristics are shown. In this case, the speed reference was changed from 35 r/min to 1500 r/min with a torque variation range from −100% (regenerative operation) through 0% (no load) to 100% (motoring operation) and the steady state maximum speed error

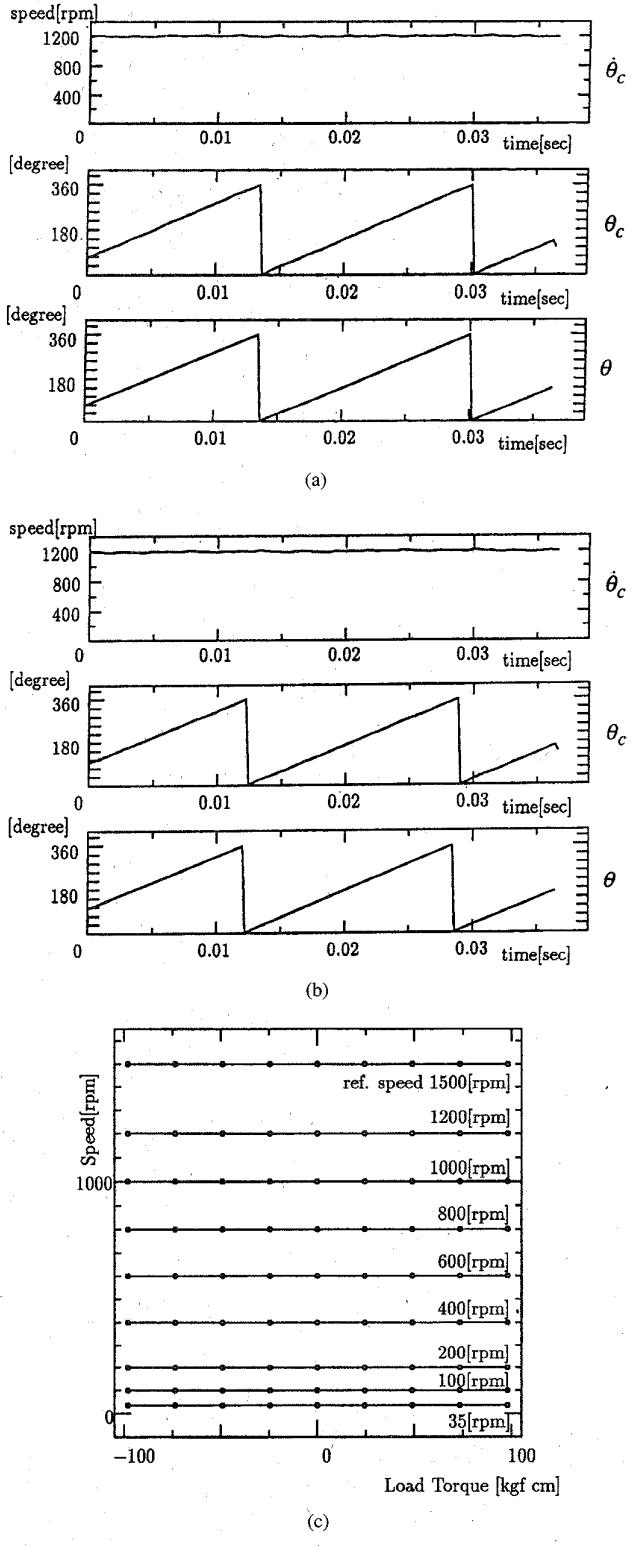

Fig. 5. Steady-state operating characteristics under current model-based control. (a) Estimated position and speed for $K_{EM} = K_E$. (b) Estimated position and speed for $K_{EM} = 1.25K_E$. (c) Torque-speed characteristics.

was within 0.4%. The speed above 1500 r/min was not obtained because of a voltage saturation of the inverter. As previously explained, the current model-based control does not use voltage information and the minimum attainable stable speed could be lower, compared to that of the voltage model-based control.

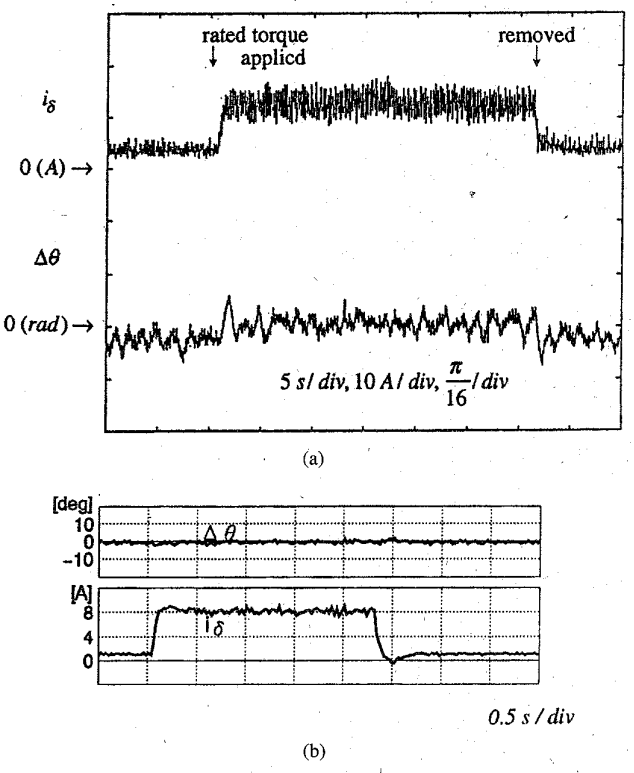

Fig. 6. Variation of $\Delta\theta$for stepwise load change. (a) Voltage model-based control. (b) Current model-based control.

Stability analysis of sensorless drives is a very important problem but a general theoretical proof of stability is very difficult. Instead, the experimental stability studies were examined. Fig. 6 shows variations of $\Delta\theta$ for the rated torque on/off condition, where (a) is obtained under the voltage model-based control and (b) is obtained under the current model-based control.

VII. Starting Procedure

As previously explained, a starting procedure for the sensorless drives of a PM brushless motor is difficult because the rotor is "active." The followings are the possible starting procedures for the PM brushless dc motors:

1) auxiliary sensor;
2) open loop control [11];
3) specific gate pattern [12];
4) arbitrary starting [9], [10];
5) salient-pole motor [13].

To identify the initial rotor position, low cost auxiliary sensors can be used. These sensors, such as small Hall devices, can provide the rotor position at standstill.

Open loop control is briefly explained in the Introduction of this paper, where the motor is started by an open loop control till the speed comes to a certain speed at which the rotor position estimation is possible.

Starting by a specific gate pattern is as follows. First, a specific gate pattern (e.g., a U-phase upper transistor, V- and W-phase lower transistors are conducting) is given to an inverter for a very short time and this is repeated several times. This means the inverter acts as a chopper with a very small duty factor. This aligns the axis in the direction of axis determined by a given specific gate pattern. (For example, the rotor axis is aligned in the direction of U-phase winding for a given gate pattern above.) Once an initial rotor position is set, the starting is possible by the proposed sensorless control algorithm.

Arbitrary starting may be done with an arbitrary gate pattern but, in some cases, may be accompanied with a temporary reverse rotation. In the extreme case, a stable start cannot be achieved.

Fig. 7 shows the typical starting characteristics by (3) and (4) under the current model-based control. In Fig. 7(a), the initial angular error is zero by a specific gate pattern and a smooth acceleration is obtained. In Fig, 7(b), the initial angular error is as large as 180° and the motor rotates in the wrong direction at first. However, as the angular error converges to zero, the motor accelerates in the desired direction.

VIII. Starting of Salient-Pole PM Brushless Motor [13]

Since the winding inductances of a salient-pole PM brushless motor are functions of the rotor position, a novel approach to estimation of the rotor position at standstill can be considered.

Suppose the case where the motor is at standstill and the specific gate pattern (again, U-phase upper transistor, V- and W-phase lower transistors are conducting) is given. In this case, (21) is obtained by rearranging the well-known voltage equation of a salient-pole PM synchronous motor [13], [14]. This relation, valid for the motor whose magnetic circuit is not saturated, means that a current gradient is a function of the rotor position

$$\frac{di_U}{dt} = \frac{4}{9}\frac{L_{g0} + L_{g2}\cos 2\theta}{L_{g0}^2 - L_{g2}^2} V_{UV}. \tag{21}$$

To examine the effect of magnetic saturation, two kinds of pilot voltages are provided as shown in Fig. 8(a). The first pilot voltage is a rectangular dc voltage pulse supplied from an inverter. The voltage is obtained by operating an inverter as a chopper with small duty. The second pilot voltage is also a voltage pulse with longer duty. The flux due to this voltage pulse is superimposed to the permanent magnet flux. The flux due to the first pilot voltage may not cause a magnetic saturation. In this case, a current gradient is given in (21) and the current amplitude distribution is obtained as in Fig. 8(b). However, the second pilot voltage causes a magnetic saturation at $\theta = 0$ because the flux is added to the permanent magnet flux at $\theta = 0$ and is subtracted from it at $\theta = \pi$. As a result, the inductance at $\theta = 0$ is smaller than that at $\theta = \pi$ due to magnetic saturation. For this reason, the current amplitude distribution for the second pilot voltage is given as in Fig. 8(c).

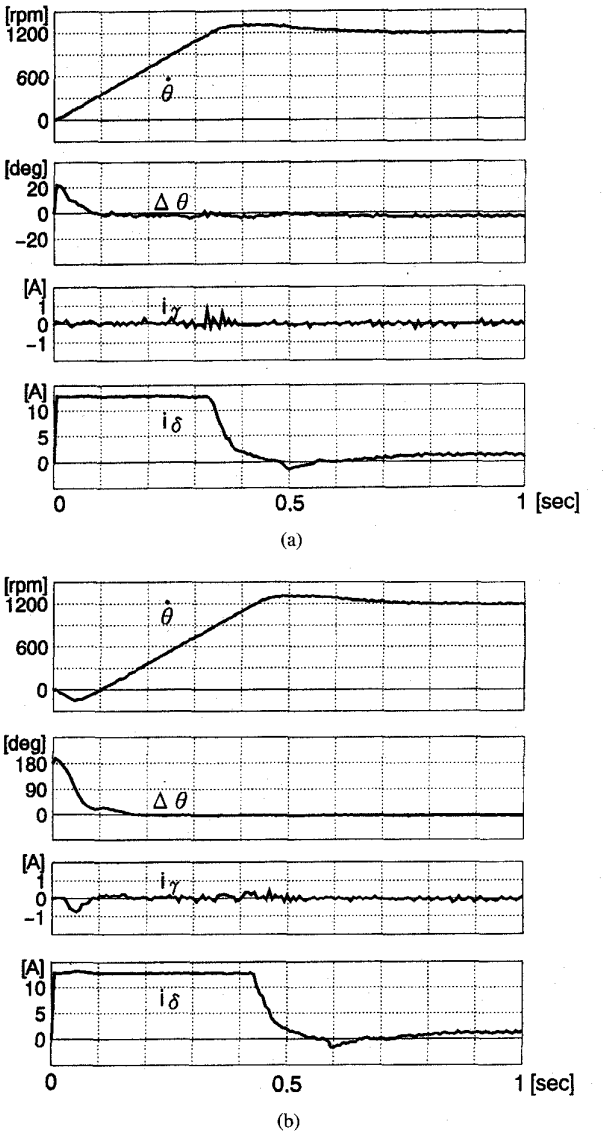

Fig. 7. Typical starting characteristics. (a) $\Delta\theta = 0°$. (b) $\Delta\theta = 180°$.

From Fig. 8(b), the following important fact can be deduced. Under the ideal case where the current amplitude distribution is a sinusoidal function of the rotor position, the amplitude of line currents are given in (22)

$$\begin{aligned} I_U &= I_o + \Delta I_U = I_o + \Delta I_o \cos 2\theta \\ I_V &= I_U + \Delta I_V = I_o + \Delta I_o \cos(2\theta + 2\pi/3) \\ I_W &= I_v + \Delta I_W = I_o + \Delta I_o \cos(2\theta - 2\pi/3) \end{aligned} \tag{22}$$

and I_o can be obtained as in (23)

$$I_o = \frac{1}{3}(I_U + I_V + I_W) \tag{23}$$

from which ΔI_U can be obtained. By referring to Fig. 8(b) and the signs of ΔI_U, ΔI_V, and ΔI_W, the relation between the rotor position and the combination of signs of ΔI can be summed up as in Table II.

As Table II shows, a combination of signs gives two domains of θ, π-radian apart from each other. To distinguish θ

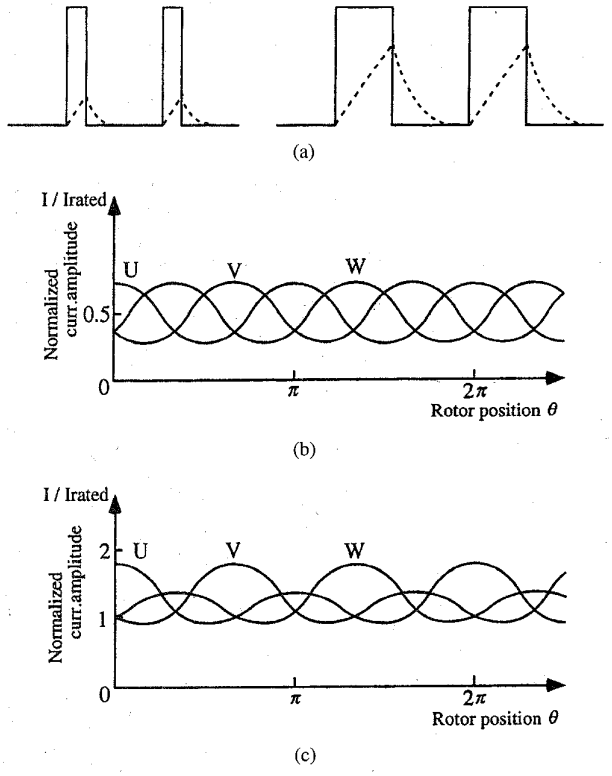

Fig. 8. Pilot voltages and current amplitude distribution. (a) Pilot voltage profiles. (b) Current amplitude distribution for pilot voltage with short duty. (c) Current amplitude distribution for pilot voltage with longer duty.

from $\theta+\pi$, the characteristics in Fig. 8(c) can be used because the current amplitude is different at θ and $\theta+\pi$. Once the domain is specified, the rotor position in $(\Delta I_U, \Delta I_V, \Delta I_W) = (+,-,-)$, for example, can be calculated by (24) and (25) under the assumption in (26)

$$\theta = \frac{\sqrt{3}(\Delta I_W - \Delta I_V)}{2(2\Delta I_U - \Delta I_V - \Delta I_W)} \quad \left(-\frac{\pi}{12} < \theta < \frac{\pi}{12}\right) \tag{24}$$

$$\theta = \pi + \frac{\sqrt{3}(\Delta I_W - \Delta I_V)}{2(2\Delta I_U - \Delta I_V - \Delta I_W)} \quad \left(\frac{11\pi}{12} < \theta < \frac{13\pi}{12}\right) \tag{25}$$

$$\theta \cong \frac{1}{2}\tan 2\theta. \tag{26}$$

The pilot voltage is a dc voltage which is applied from an inverter and the current peak is measured through a current sensor. For example, the gate pattern (U^+, V^-, W^-) is provided for the detection of U-phase current peak. Similarly, the gate patterns (V^+, W^-, U^-) and (W^+, U^-, V^-) are provided to detect V-phase and W-phase current peaks, respectively. By comparing these current peaks, the initial rotor position may be deduced as θ or $\theta+\pi$. To distinguish between θ and $\theta+\pi$, another pilot voltage with longer duty is applied in a similar manner. Among the three windings, the nearest winding to N-pole presents higher current peak than the others and θ and $\theta+\pi$ can be discriminated.

Fig. 9(a) shows the experimental current waveforms, where the first three current responses are obtained for the pilot voltages (U^+, V^-, W^-), (V^+, W^-, U^-), and (W^+, U^-, V^-) with shorter duty factor, respectively, and the fourth current response is obtained for (U^+, V^-, W^-) with longer duty factor. The current amplitude-rotor position characteristics for pilot voltages with shorter and longer duties are given in Fig. 9(b) and (c). Fig. 10 shows a relation between the actual initial rotor position and the estimated position. It is noted here that close agreement between the estimated initial position and the actual one has been obtained. This means that the stable and smooth starting is possible under the sensorless control algorithm. The small deviation of experimental results is due to the fact that the current distribution in Fig. 9(b) and (c) is not strictly sinusoidal.

TABLE II
COMPARISON OF CHARACTERISTICS

θ	ΔI_U	ΔI_V	ΔI_W
$-\frac{\pi}{12} \sim \frac{\pi}{12}$ $\frac{11\pi}{12} \sim \frac{13\pi}{12}$	+	−	−
$\frac{\pi}{12} \sim \frac{\pi}{4}$ $\frac{13\pi}{12} \sim \frac{5\pi}{4}$	+	−	+
$\frac{\pi}{4} \sim \frac{5\pi}{12}$ $\frac{5\pi}{4} \sim \frac{17\pi}{5}$	−	−	+
$\frac{5\pi}{12} \sim \frac{7\pi}{12}$ $\frac{17\pi}{5} \sim \frac{19\pi}{12}$	−	+	+
$\frac{7\pi}{12} \sim \frac{3\pi}{4}$ $\frac{19\pi}{12} \sim \frac{7\pi}{4}$	−	+	−
$\frac{3\pi}{4} \sim \frac{11\pi}{12}$ $\frac{7\pi}{4} \sim \frac{23\pi}{12}$	+	+	−

IX. COMPARISON OF CONTROL CHARACTERISTICS

Table III shows a comparison of the proposed voltage model-based and the current model-based control characteristics. In the voltage model-based control, the hypothetical speed in (7) is calculated every sampling and, therefore, high accuracy is required in the calculation of v_δ and pi_δ. For this reason, the effects of the dead time and current ripple on the accuracy of the speed estimation is serious. As previously explained, a moving average was used to avoid these effects. At the same time, a variation of K_E also gives a serious effect on the speed estimation. In this sense, the method is not robust against parameter variations. To solve this disadvantage, a parameter identifier proposed by the authors is effective [15].

In the current model-based control, the estimated position and speed are corrected every sampling by a current error between the detected and estimated values. As a result, the estimation is more stable than that of the voltage model-based control.

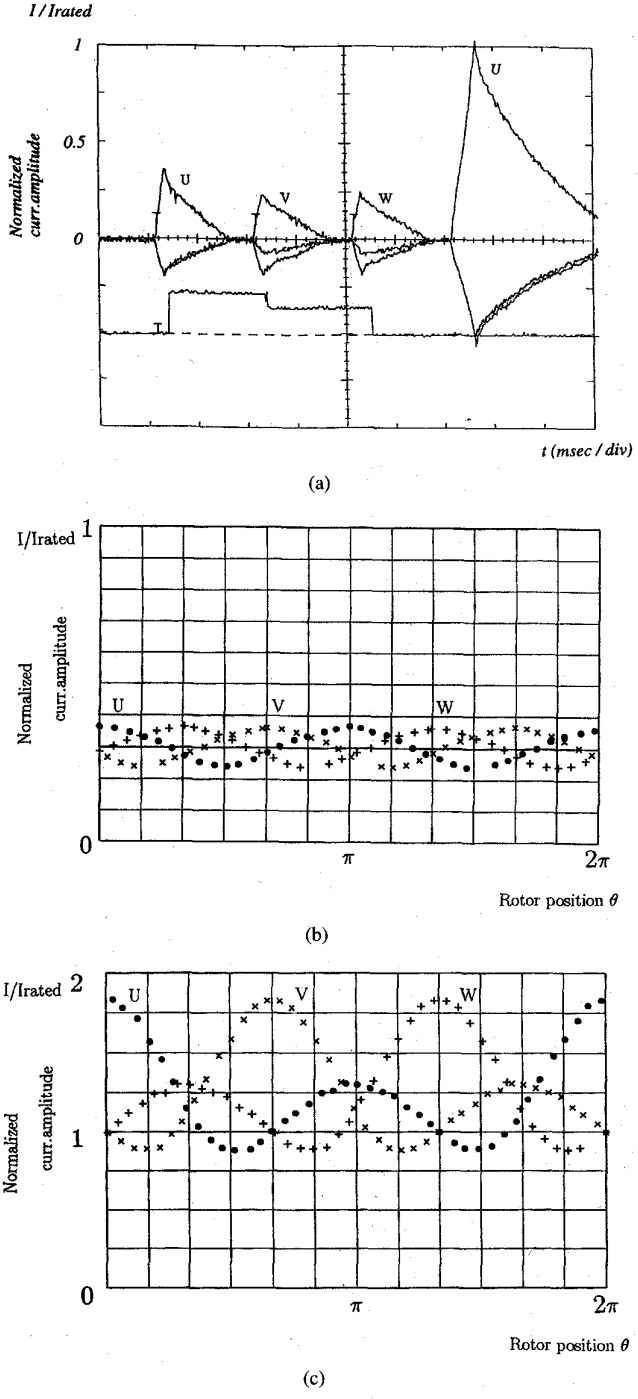

Fig. 9. Experimental results. (a) Experimental current waveforms. (b) Current distribution (short duty). (c) Current distribution (long duty).

X. Conclusion

From standpoints of size, cost reduction, maintenance, and reliability, the elimination of position and speed sensors is desired. For this purpose, two approaches have been explained and tested for the brushless motor with a sinusoidal flux distribution. One is based on the voltage model of a brushless motor and another on the current model. The basic idea of estimating the position and speed is to use the difference between the actual state variables and the estimated state variables. In the sensorless control, the starting procedure is also a problem. Since no information is available before a starting, the self-starting is theoretically impossible. Some approaches are reviewed and a novel initial position estimation for a salient-pole PM brushless dc motor is explained. The method is based on the position dependency of winding inductance.

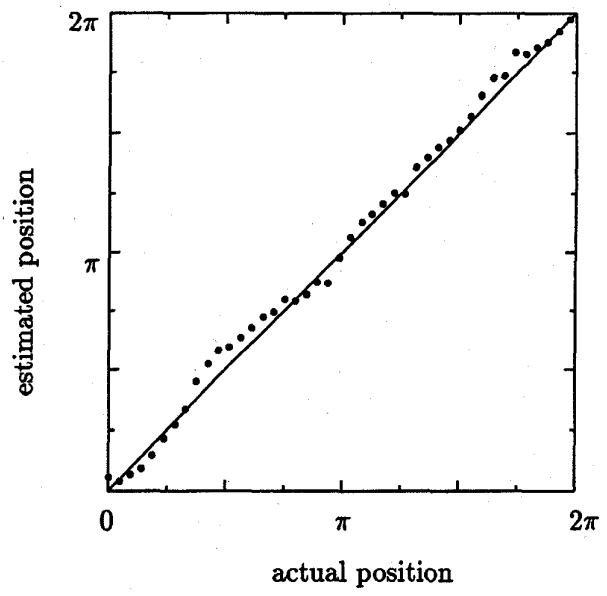

Fig. 10. Actual and estimated rotor position at standstill.

TABLE III
Relation Between Rotor Position and Signs of ΔI

	Voltage model-based	Current model-based
Estimation	Based on voltage error	Based on current error
Equation	Voltage equation	Current equation
Starting	By specific PWM pattern	By specific PWM pattern
Min. speed	100 rpm	35 rpm
Accuracy of speed cont'l	Less than 1 %	Less than 0.4 %
Parameter variation	Need of parameter identifier	Robust

Acknowledgment

The author would like to thank M. A. Rahman, the Guest Editor, for giving him the chance to write this paper.

References

[1] P. Ferraris, A. Vagatti, and F. Villate, "PM brushless motor drives: A self-commutating system without rotor-position sensors," in *Proc. 9th Annu. Symp. Incremental Motion Contr. Syst., Devices*, June 1980, pp. 305–312.
[2] K. Iizuka *et al.*, "Microcomputer control for sensorless brushless motor," *IEEE Trans. Ind. Applicat.*, vol. IA-21, pp. 595–601, May/June 1985.
[3] M. D. Erdman, H. B. Harms, and J. L. Oldenkamp, "Electronically commutated DC motor for the appliance industry," in *IEEE-IAS Conf. Rec.*, 1984, pp. 1339–1345.
[4] R. B. Sepe and J. H. Lang, "Real-time observer-based control of a permanent-magnet synchronous motor without mechanical sensor," in *IEEE-IAS Conf. Rec.*, 1991, pp. 475–481.

[5] S. Ogasawara and H. Akagi, "An approach to position sensorless drive for brushless DC motor," in *IEEE-IAS Conf. Rec.*, 1990, pp. 443–447.
[6] T. H. Liu and C. P. Cheng, "Adaptive control for a sensorless permanent-magnet synchronous motor drive," in *IEEE-IAS Conf. Rec.*, 1992, pp. 413–418.
[7] L. A. Jones and J. H. Lang, "A state observer for permanent magnet synchronous motor," *IEEE Trans. Ind. Electron.*, vol. 36, no. 3, pp. 374–382, 1989.
[8] S. Bolognani, R. Oboe, and M. Zigliotto, "DSP-based extended Kalman filter estimation of speed and rotor position of a PM synchronous motor," in *Proc. IECON '94*, 1994, pp. 2907–2107.
[9] N. Matsui, "Sensorless operation of brushless DC motor drives," in *Proc. IECON '93*, 1993, pp. 739–744.
[10] N. Matsui, T. Takeshita, and K. Yasuda, "A new sensorless drive of brushless DC motor," in *Proc. IECON '92*, 1992, pp. 430–435.
[11] R. Wu and G. R. Slemon, "A permanent magnet motor drive without a shaft sensor," *IEEE Trans. Ind. Applicat.*, vol. 27, no. 5, pp. 1005–1011, Sept./Oct. 1991.
[12] N. Matsui and M. Shigyo, "Brushless DC motor control without position and speed sensors," *IEEE-IAS Conf. Record*, 1990, pp. 448–454.
[13] N. Matsui and T. Takeshita, "A novel starting method of sensorless salient-pole brushless motor," *IEEE IAS Conf. Rec.*, 1995, pp. 386–392.
[14] A. E. Fitzgerald and C. Kingsley, *Elec. Machinery*. New York: McGraw-Hill Company.
[15] N. Matsui and H. Ohashi, "DSP-based adaptive control of a brushless motor," in *IEEE-IAS Conf. Rec.*, 1988, pp. 375–380.

Nobuyuki Matsui was born in Wakayama, Japan, on May 7, 1943. He received the B.S. and M.S. degrees in electrical engineering from Nagoya Institute of Technology, Nagoya, Japan, in 1966 and 1968, respectively, and the Ph.D. degree from the Tokyo Institute of Technology, Tokyo, Japan, in 1976.

Since 1968, he has been with the Department of Electrical and Computer Engineering, Nagoya Institute of Technology, where he is currently a Professor and is engaged in research on computer control of electrical motors.

Dr. Matsui is a member of the Institute of Electrical Engineers of Japan (IEEJ), the Society of Instrumentation and Control Engineers (SICE), and the Robotic Society of Japan (RSJ).